Magnetic moments of chiral phonons induced by coupling with magnons

Qian Wang, Meng-Qiu Long,* and Yun-Peng Wang†
Hunan Key Laboratory for Super-Micro Structure and Ultrafast Process, School of Physics, Central South University, 932 South Lushan Road, Changsha, People's Republic of China

(Received 4 January 2024; revised 21 May 2024; accepted 1 July 2024; published 17 July 2024)

Chiral phonons composed of circular atomic motion possess a tiny magnetic moment as a result of the small g factor of ions. The couplings with the spin and orbit of electrons could entail a large magnetic moment. In this paper, we explore the possibility of an emergent phonon magnetic moment due to coupling with magnons in a hexagonal lattice. The magnetic moment of the phonon results from the mixture of magnon composition in the nonresonant coupling condition. Only one of the optical phonons gains a magnetic moment in the ferromagnetic case, while both phonon modes acquire a magnetic moment in the antiferromagnetic case. The magnon-induced magnetic moment of the phonon is proportional to the square of the magnon-phonon coupling strength. We also studied the case of nonequal atomic masses on sublattices which entails different magnetic moments of the two phonon modes.

DOI: 10.1103/PhysRevB.110.024423

Phonons are quasiparticles corresponding to the collective motions of atoms in crystals. Phonons are traditionally regarded as linear back-and-forth atomic motions, thus possessing no angular momentum. It was not until the proposal of chiral phonons [1–3] that people recognized the concept of angular momentum of phonons. Chiral phonons, i.e., circularly polarized phonons carrying finite angular momentum, have been validated in several material systems like $Fe_2Mo_3O_8$, WSe_2, and α-HgS [4–7]. The angular momentum of phonons plays a crucial role in the Einstein–de Haas effect [8] and Barnett effect [9]. The phonon angular momentum has been demonstrated to play a significant role in the magnon-phonon coupling [10–13]. Circular rotations of charge-carrying ions generate magnetic moments [14,15]. The magnetic moments of phonons are smaller than those of electrons by a factor of the mass ratio between an ion and an electron. The calculated magnetic moments of phonons are on the order of 10^{-3} μ_B or less [16–18].

A large phonon magnetic moment on the order of μ_B has been identified in nonmagnetic and paramagnetic materials [19–22]. The large magnitude of phonon magnetic moments cannot be attributed to solely the circular motions of ions [17]; instead the interactions with the spin of conducting electrons play a dominant role [18]. The chiral phonons possessing angular momentum interact with the spin of conducting electrons [7,23]. Theory and experiment observed the angular momentum transfer between phonons and magnons [24–26]. The transient chiral phonon in $KTaO_3$ acquires a magnetic moment of 0.1 μ_B due to coupling with electron spin [27]. The coupling with cyclotron motion of electrons results in a giant magnetic moment of 2.7 μ_B in Dirac semimetallic Cd_3As_2 [19]. A quantum mechanical theory of phonon magnetic moments has been developed in which the adiabatic correction to electronic wave functions dominates over the contributions of momentum-resolved Born effective charges [28–30].

The coherent hybridization with magnons is another mechanism for phonons to acquire a magnetic moment [31]. Magnon polarons [32–37] emerging from strong magnon-phonon coupling have mixed characteristics in normal modes. The phonon-dominated modes also possess a sizable magnon component which brings a finite magnetic moment. The magnetic moment of phonon is ubiquitous in magnetic materials; that is, there is no symmetry requirement for the emergent phonon magnetic moment. A sizable magnetic moment of phonons only requires a sizable magnon-phonon coupling strength. We anticipate that magnetic materials with active orbital degrees of freedom, such as $FePS_3$ and $Fe_2Mo_3O_8$, probably possess strong magnon-phonon coupling, hence large phonon magnetic moments. We chose the hexagonal lattice as the model because materials with strong magnon-phonon coupling usually have a hexagonal lattice. We also discuss the existence of phonon magnetic moments in kagome and square lattices; this discussion is in the Supplemental Material [38].

In this paper, we introduce a model to demonstrate the mechanism responsible for the magnon-induced phonon magnetic moments. A simple hexagonal lattice model was utilized to demonstrate the consequence of selective magnon-phonon coupling on the magnitude of phonon magnetic moments.

A two-dimensional hexagonal lattice carries magnons and phonons which are coupled with each other. We assume the electronic orbital degree of freedom is frozen. The Hamiltonian [39–41] consists of three parts, namely the spin, lattice, and magnetoelastic coupling,

$$H = H_m + H_p + H_{mp}. \quad (1)$$

*Contact author: mqlong@csu.edu.cn
†Contact author: yunpengwang@csu.edu.cn

The spin Hamiltonian reads

$$H_m = -J\sum_{\langle i,j\rangle}\mathbf{S}_i\cdot\mathbf{S}_j - J_z\sum_{\langle i,j\rangle}S_i^zS_j^z - B_z\sum_i S_i^z. \quad (2)$$

The first term represents the isotropic Heisenberg exchange with the strength of J, where $J>0$ prefers the ferromagnetic (FM) state, but $J<0$ prefers the antiferromagnetic (AFM) state. The second term stands for the uniaxial anisotropic exchange with the strength of $J_z>0$ which favors out-of-plane spins, while the last term is the effect of an external magnetic field B_z along the z direction.

The Hamiltonian describing the lattice vibrations reads

$$H_p = \frac{m}{2}\sum_i \mathbf{v}_i^2 + \frac{k}{2}\sum_{\langle i,j\rangle}(\mathbf{u}_i-\mathbf{u}_j)^2, \quad (3)$$

where m is the atomic mass and k is the elastic constant among neighboring atoms. $\mathbf{u}_i$ and $\mathbf{v}_i$ are respectively the displacement and the velocity vector of the ith atom. We ignore the out-of-plane vibrations of atoms since these modes are not coupled with magnons.

The spin-lattice coupling bilinear in terms of the spin and the displacement is expressed as

$$H_{mp} = \lambda\sum_i\sum_e[(\mathbf{S}_i\cdot\mathbf{e})(u_i-u_{i+e})]. \quad (4)$$

This form was proposed by Kittel [42,43], and was also adopted in recent works [39–41], where λ is the magnon-phonon coupling strength and $\mathbf{e}$ refers to the three unit vectors connecting one atom to its three nearest neighbors.

The linearized equation of motion [44,45] for magnon and phonon in the classical regime is

$$\frac{d}{dt}\begin{pmatrix}V\\U\\S\end{pmatrix} = \begin{pmatrix}F/m\\V\\T\end{pmatrix} = \begin{pmatrix}0 & \boldsymbol{D} & \boldsymbol{A}\\ 1 & 0 & 0\\ 0 & \boldsymbol{B} & \boldsymbol{C}\end{pmatrix}\cdot\begin{pmatrix}V\\U\\S\end{pmatrix}; \quad (5)$$

here V, U, and S are the velocities, displacements, and local magnetic moments; F and T refer to the forces on atoms and torques on spins. $\boldsymbol{D}\equiv d(F/m)/dU$ is the force-constant matrix, and $\boldsymbol{C}\equiv dT/dS$ describes the spin-spin interaction. $\boldsymbol{A}\equiv d(F/m)/dS$ and $\boldsymbol{B}\equiv dT/dU$ stand for the spin-lattice coupling. The equation of motion derived by Ren *et al.* [45] has a quite similar form, except they also considered the Berry curvature such that the dependence on atomic velocity is nonzero. The Berry curvature terms involve the electronic degree of freedom; they are ignored in our method. The spectra of magnon and phonon modes are solved using the method of equations of motion in our previous work [10,46].

Figure 1 shows the calculated dispersion relations of magnons and phonons in a hexagonal lattice. The magnon and phonon band structure with the magnon-phonon coupling is illustrated in Fig. 1(a) for the AFM case. An external magnetic field along the z direction with $B_z=0.01J$ splits the degenerate magnon. According to their normal modes, the two magnon bands are labeled as M_R and M_L, respectively. There are four phonon bands (the blue line), and two acoustic and two optical phonon bands since the out-of-plane vibrations are not considered. The two optical phonon bands are degenerate at the Γ point when magnon-phonon coupling is turned off $\lambda=0$. Once the magnon-phonon coupling is turned on, an

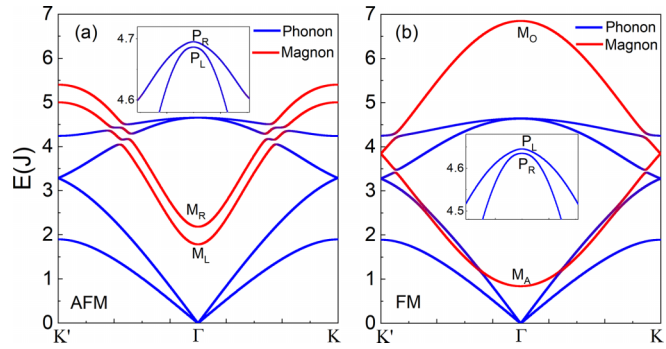

FIG. 1. Calculated magnon-phonon dispersion relation in (a) the antiferromagnetic and (b) the ferromagnetic configurations. The anisotropic exchange strength is set to $J_z=0.1J$, coupling strength is $\lambda=0.01J$, and the external magnetic field $B_z=0.01J$. The characteristics of normal modes are represented by pseudocolors: red for pure magnons and blue for pure phonons.

anticrossing feature emerges where the uncoupled magnon and phonon bands cross each other. These anticrossings are characteristics of the resonant coupling between magnon and phonon [10].

Moreover, the originally degenerated optical phonon bands at the Γ point are lifted in the presence of magnon-phonon coupling, as illustrated in Fig. 1(a) and its inset. They split into two chiral phonons moving in opposite directions, labeled P_R and P_L. Note that the splitting of optical phonons only occurs under magnetic fields. The splitting of optical phonons at Γ is different from the above-mentioned band anticrossing; in fact these phonons at Γ are in the nonresonant condition with magnons with a large frequency difference. For the case of FM, there are two nondegenerated magnon modes corresponding to the in-phase and out-of-phase precessions of spins at the two sublattices. The frequency of the acoustic magnon (denoted as M_A) at Γ is nonzero due to the magnetic anisotropy of $J_z=0.1J$. The optical magnon is denoted as M_O shown in Fig. 1(b).

When coupled with the magnon, the two optical phonon bands are no longer degenerate at the Γ point, as illustrated in Fig. 1(b) with $\lambda=0.01J$. The splitting of degenerated optical phonons at the Γ point again results from nonresonant coupling with magnons. As will be discussed later, through magnon-phonon coupling, magnons contaminate the two phonon modes by different degrees, which causes phonon splitting. The contamination by magnons introduces magnetic moments to the phonon modes. Hereafter, we will focus on the magnon and phonon modes at the Γ point, which could be observed using the Raman spectra [47,48].

We apply a magnetic field along the z direction and observe frequency shifts of the magnons and the phonons modes at the Γ point. The shifts in the frequency of a quasiparticle due to magnetic fields can be attributed to its magnetic moment. For the case of AFM, the frequency of magnon mode M_R increases while the frequency of M_L decreases, as illustrated in Fig. 2(a). This is because the two AFM resonance modes possess magnetic moments with opposite directions.

The frequencies of optical phonon modes also shift under magnetic field. At $B_z=0$ the two optical phonons are

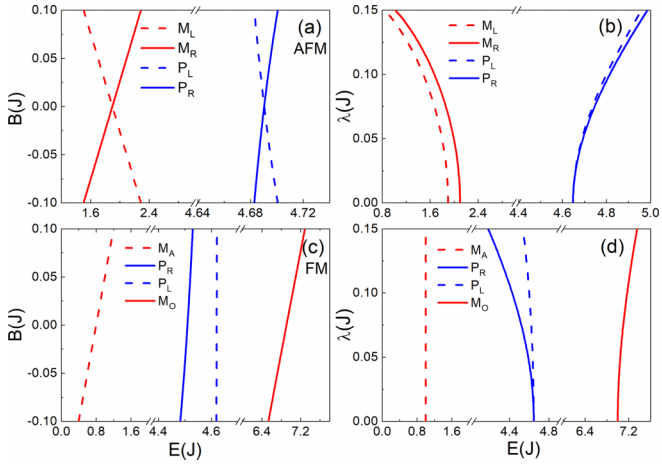

FIG. 2. The frequency of magnons and phonons under the external magnetic field and the coupling strength at the Γ point. (a) The frequency splitting of the two pairs of AFM magnons and phonons with $\lambda = 0.05J$. (b) The energy as a function of the coupling strength with $B_z = 0.02J$ in AFM. (c) and (d) are the frequency changes of magnons and phonons in the case of FM.

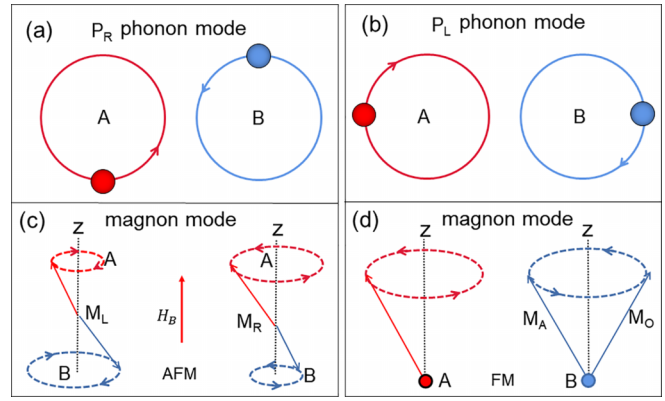

FIG. 3. Sublattice polarizations of phonon and magnon modes in AFM and FM at the Γ point. The hexagonal lattice has two atoms A and B represented in red and blue, respectively. (a) P_R is a right-handed phonon, and the angular momentum of the phonon is $+1$. (b) P_L is a left-handed phonon that has a phonon angular momentum of -1. (c) M_R is a right-handed magnon with the magnon angular momentum of $+1$ and M_L is a left-handed magnon in AFM with the magnon angular momentum of -1. (d) M_A is the acoustic magnon mode, and M_O is optical magnon mode in FM.

degenerate, but their frequencies shift in opposite directions under magnetic field; see Fig. 2(a). The frequency shift is linear with respect to the magnetic field. Therefore one can assign well-defined magnetic moments to these optical phonon modes; their magnetic moments therefore have opposite signs.

One can calculate the magnetic moments of magnons and phonons from the slope of their frequencies with respect to the magnetic field. For instance, at magnon-phonon coupling strength of $\lambda = 0.05J$, the calculated magnetic moments of magnons are reduced from $\pm 2\ \mu_B$ to $\pm 1.95\ \mu_B$ while the optical phonons have magnetic moments of $\pm 0.05\ \mu_B$.

The situation of frequency shifts in the FM case is different from the aforementioned AFM case, as illustrated in Fig. 2(c). The frequencies of both acoustic magnon M_A and optical M_O shift linearly as the magnetic field increases, because the two FM resonance modes possess the same magnetic moment of about $2\ \mu_B$. For the two optical phonon modes, one of them, denoted as P_R, shifts to higher frequency as the magnetic field increases, while the frequency of the other, denoted as P_L, remains unchanged. Therefore, the phonon mode P_R has a finite magnetic moment, while P_L is not magnetic.

In order to understand the different magnetic moments of phonons in the FM case, we tune the magnon-phonon coupling strength and trace the evolution of the frequencies of magnon and phonon modes. When one magnon mode is coupled with a phonon, their frequencies would repulse each other; as the coupling strength increases, the degree of repulsion is enhanced. As shown in Fig. 2(d), the M_A magnon and the P_L phonon are almost inert. Therefore, the acoustic magnon M_A is not coupled to any phonon; the P_L phonon is not coupled to any magnon. The other two modes, namely the optical phonon P_R and optical magnon M_O, repulse each other, so they are coupled. Now we can understand the different magnetic moments of phonon modes P_L and P_R. The phonon P_L is not coupled with any magnon so it has no magnetic moment; instead the phonon P_R is coupled with magnon M_O so it has a finite magnetic moment.

The repulsion among magnon and phonon in the AFM case is also illustrated in Fig. 2(b). Under a finite magnetic field of $B_z = 0.02J$, both AFM magnons shift to lower frequencies and both phonons shift to higher frequencies as the magnon-phonon coupling becomes stronger. The frequency curves of both magnons are nearly parallel; thus their effective coupling strengths with phonons are nearly the same. The same effective coupling strength also explains the same magnitude of magnetic moments of the two phonons. The magnon-phonon coupling requires the matching of their angular momenta [10,11]. A magnon and a chiral phonon are effectively coupled if their normal modes rotate along the same direction. The selective coupling between magnon and phonon can be understood by examining their normal modes shown in Fig. 3. Both optical phonon modes are composed of circular motions of atoms and there is a π-phase difference between sublattices. Atoms rotate in the clockwise manner for the P_L mode, while counterclockwise for the P_R mode, as illustrated in Figs. 3(a) and 3(b). For the magnon mode M_L in the AFM case, the in-plane component of local magnetic moments rotates in a clockwise manner [see Fig. 3(c)]; it is consistent with that of the phonon P_L mode, but opposite to P_R. As discussed in our previous work [10], phonons and magnons with opposite motion directions fail to couple with each other. Therefore the magnon M_L only couples with phonon P_L but not P_R. Similarly, the magnon M_R couples with phonon P_R but is not coupled with P_L.

The situation of magnon-phonon coupling for the FM case is in strong contrast to the AFM case discussed above. The local magnetic moments for the acoustic magnon mode (M_A) rotate in-phase, that is, without phase difference between sublattices. Therefore, the acoustic magnon is not coupled with optical phonons which have a π-phase difference between sublattices. On the other hand, the optical magnon mode (M_O)

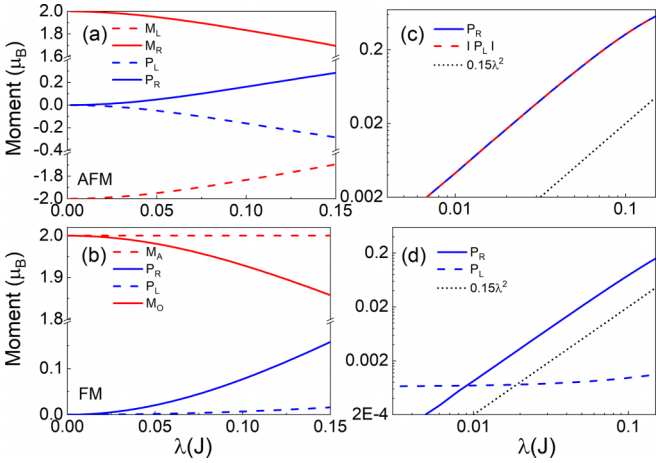

FIG. 4. Magnetic moments at (a) AFM and (b) FM. The phonon magnetic moment and coupling strength for AFM (c) and FM (d) with a log-log scale. Here the magnon magnetic moment is shown in red, and the phonon magnetic moment is shown in blue.

has a π-phase difference, so it is allowed to couple with the optical phonon mode. However, the local magnetic moments in the optical magnon mode rotate in a counterclockwise manner, so it couples only with the P_R phonon mode but not P_L.

A phonon carrying a finite magnetic moment exhibits the phonon Zeeman effect; that is, its frequency shifts linearly with the magnetic field: $\delta\omega = \mu \cdot \delta B_z$. The phonon Zeeman effect thus provides a direct way to measure the phonon magnetic moment [31]. The magnetic moments of phonon modes can be calculated from the dependence of their frequencies on the magnetic field. In practice, we employ the finite-difference method to calculate $\mu = \Delta\omega/\Delta B_z$. The calculated magnetic moments of magnons and phonons are plotted in Fig. 4 as a function of the magnon-phonon coupling strength λ. For the AFM case [Fig. 4(a)], the magnetic moments of magnons M_L and M_R are $\mp 2\ \mu_B$ in the absence of magnon-phonon coupling. As the coupling strength λ increases, the magnitude of the magnetic moment of the M_R magnon decreases, and so does the M_L magnon. At the same time, the magnetic moment of phonon modes P_R and P_L emerges and increases as λ is enhanced. At $\lambda = 0.15J$, the phonon modes M_L and M_R possess a magnetic moment of about $0.3\ \mu_B$.

Our data also show that the sum of magnetic moments of M_L and P_L remains $2\ \mu_B$ irrespective of the λ, and so does the sum of magnetic moments of M_R and P_R. This result can be interpreted as a transfer of the magnetic moments from magnon M_L (M_R) to phonon P_L (P_R) intermediated by the magnon-phonon coupling. The magnetic moment transfer explains the reduction in the magnon magnetic moment and the enhancement in the phonon magnetic moment, which entails the conservation of the total magnetic moment of magnon-phonon pairs M_L-P_L and M_R-P_R.

The nonlinear relation between magnetic moments and the magnon-phonon coupling strength λ as illustrated in Fig. 4 can be understood using a two-level system model. According to the previous analysis, we only need to consider one magnon mode coupled with another phonon mode. The Hamiltonian of this magnon-phonon two-level system can be expressed by a 2×2 matrix,

$$H_{\text{eff}} = \begin{pmatrix} E_p^0 & \lambda_0 \\ \lambda_0 & E_m^0 - \mu B_z \end{pmatrix}, \tag{6}$$

where E_p^0 and E_m^0 are the energies of phonon and magnon modes in the absence of coupling; the magnon mode gains an extra energy $-\mu B_z$ due to the magnetic field B_z; here $\mu = 2\ \mu_B$ refers to the magnetic moment of a bare magnon. The magnon and phonon is coupled and the effective coupling strength $\lambda_0 = 4\lambda$ in Eq. (4). In the following we treat λ_0 as a small quantity with respect to $|E_m^0 - E_p^0|$. The eigenvalues of H_{eff} give the energies of the phonon and magnon, whose derivative over magnetic field B_z gives the magnetic moments. The magnetic moment of the magnon at $B_z = 0$ is

$$\mu_m \approx \mu - \mu\lambda_0^2/\Delta^2, \tag{7}$$

where $\Delta = |E_m^0 - E_p^0|$. This result indicates that the magnetic moment of a magnon is always reduced by coupling with a phonon; this is what we have seen in Figs. 4(a) and 4(b).

The magnetic moment of the phonon at $B_z = 0$ is

$$\mu_p \approx \mu\lambda_0^2/\Delta^2. \tag{8}$$

This indicates that the magnetic moment of the phonon is always parallel to that of the coupled magnon. Combining Eq. (7) and Eq. (8), one can obtain $\mu_p + \mu_m = \mu$; that is, the sum of magnetic moments of a coupled pair of magnon and phonon is always equal to that of a bare magnon. Equation (8) also indicates that the phonon magnetic moment is proportional to the square of the coupling strength. The calculated phonon magnetic moment versus coupling strength λ_0 is plotted in Figs. 4(c) and 4(d) with a log-log scale. The curves in Figs. 4(c) and 4(d) are approximately straight and the slope is approximately equal to 2, consistent with the $\mu_p \propto \lambda_0^2$ relation.

Lastly, we explore the case of different atomic masses on the two sublattices. With the inversion symmetry broken, the chiral phonon modes at the K and K' points are split [2]. Interestingly, there is also a split chiral phonon at the Γ point with the magnon-phonon coupling, and the phonon magnetic moment depends on the ratio of atomic masses. We concentrate on the phonon magnetic moment at the Γ point in the AFM case. Setting the unequal atomic masses on sublattices A and B with $m_B/m_A = 0.8$ and setting coupling strength $\lambda = 0.05J$, the evolution of phonon and magnon energies with respect to the magnetic field B_z is shown in Fig. 5(a). At $B_z = 0$, the magnons are degenerate, while the two optical phonons are not degenerate with a tiny splitting. This is because the different atomic masses cause different radius of circular atomic motion, and the resulting phonon angular momentum is different, making the effective magnon-phonon coupling strength different.

According to Eq. (8), the magnetic moments of phonon modes are proportional to the square of effective coupling strength. Therefore, different magnetic moments of P_L and P_R are expected. Calculations give $-0.023\ \mu_B$ for P_L and $0.021\ \mu_B$ for P_R. As the mass ratio m_B/m_A decreases, the difference in magnetic moments of phonon modes P_L and P_R is enhanced. The ratio of phonon magnetic moments is plotted

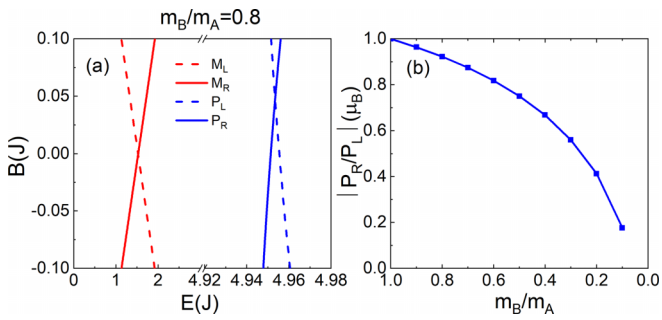

FIG. 5. Magnon-phonon coupling at different atomic masses in AFM at the Γ point. (a) Phonon and magnon frequencies as a function of the external magnetic field with $m_B/m_A = 0.8$. (b) The relationship between phonon magnetic moment of P_R/P_L and atomic masses of m_B/m_A.

in Fig. 5(b). The ratio of magnetic moments is approximately proportional to $(m_B/m_A)^2$.

In summary, we studied the emergence of magnetic moments of optical phonon modes brought up by selective coupling and hybridization with magnon modes in a hexagonal lattice model. Not all optical phonon modes gain a magnetic moment because magnon-phonon coupling is selective. The nonresonant condition entails the magnitude of phonon magnetic moment quadratic with the coupling strength. The effective coupling strength could also be tuned by changing the atomic mass on sublattices. Our results indicate that chiral phonons carrying magnetic moments can serve as an efficient carrier of spin information.

We acknowledge funding from the National Natural Science Foundation of China (Grant No. 12004439), Natural Science Foundation of Hunan Province (Grant No. 2022JJ30049), and the Hunan Province postgraduate research and innovation project (Grant No. CX20230229), and computational resources from the High Performance Computing Center of Central South University.

[1] L. Zhang and Q. Niu, Phys. Rev. Lett. **112**, 085503 (2014).
[2] L. Zhang and Q. Niu, Phys. Rev. Lett. **115**, 115502 (2015).
[3] Z. Hanyu, J. Yi, L. Ming Yang, and Z. Xiang, Science. **359**, 579 (2018).
[4] G. Grissonnanche, S. Thériault, A. Gourgout, M.-E. Boulanger, E. Lefrançois, A. Ataei, F. Laliberté, M. Dion, J.-S. Zhou, S. Pyon *et al.*, Nat. Phys. **16**, 1108 (2020).
[5] S. R. Tauchert, M. Volkov, D. Ehberger, D. Kazenwadel, M. Evers, H. Lange, A. Donges, A. Book, W. Kreuzpaintner, U. Nowak *et al.*, Nature (London) **602**, 73 (2022).
[6] K. Ishito, H. Mao, Y. Kousaka, Y. Togawa, S. Iwasaki, T. Zhang, S. Murakami, J.-i. Kishine, and T. Satoh, Nat. Phys. **19**, 35 (2023).
[7] K. Kim, E. Vetter, L. Yan, C. Yang, Z. Wang, R. Sun, Y. Yang, A. H. Comstock, X. Li, J. Zhou *et al.*, Nat. Mater. **22**, 322 (2023).
[8] A. Einstein and W. J. de Haas, KNAW Proc. **18**, 696 (1915).
[9] S. J. Barnett, Phys. Rev. **6**, 239 (1915).
[10] Q. Wang, S. Liu, M.-Q. Long, and Y.-P. Wang, Phys. Rev. B **108**, 174426 (2023).
[11] J. Cui, E. V. Boström, M. Ozerov, F. Wu, Q. Jiang, J.-H. Chu, C. Li, F. Liu, X. Xu, A. Rubio *et al.*, Nat. Commun. **14**, 3396 (2023).
[12] N. Li, R. R. Neumann, S. K. Guang, Q. Huang, J. Liu, K. Xia, X. Y. Yue, Y. Sun, Y. Y. Wang, Q. J. Li *et al.*, Phys. Rev. B **108**, L140402 (2023).
[13] D. A. Garanin and E. M. Chudnovsky, Phys. Rev. B **92**, 024421 (2015).
[14] G. Xiong, H. Chen, D. Ma, and L. Zhang, Phys. Rev. B **106**, 144302 (2022).
[15] D. M. Juraschek, T. Neuman, and P. Narang, Phys. Rev. Res. **4**, 013129 (2022).
[16] D. M. Juraschek and N. A. Spaldin, Phys. Rev. Mater. **3**, 064405 (2019).
[17] D. M. Juraschek, P. Narang, and N. A. Spaldin, Phys. Rev. Res. **2**, 043035 (2020).
[18] R. M. Geilhufe, V. Juričić, S. Bonetti, J.-X. Zhu, and A. V. Balatsky, Phys. Rev. Res. **3**, L022011 (2021).
[19] B. Cheng, T. Schumann, Y. Wang, X. Zhang, D. Barbalas, S. Stemmer, and N. P. Armitage, Nano Lett. **20**, 5991 (2020).
[20] A. Baydin, F. G. G. Hernandez, M. Rodriguez-Vega, A. K. Okazaki, F. Tay, G. T. Noe, I. Katayama, J. Takeda, H. Nojiri, P. H. O. Rappl *et al.*, Phys. Rev. Lett. **128**, 075901 (2022).
[21] D. L. Mills and S. Ushioda, Phys. Rev. B **2**, 3805 (1970).
[22] L. Jiaming, L. Tong, Z. Junjie, C. Xiaotong, R. B. Elizabeth, X. Rui, I. Y. Boris, and Z. Hanyu, Science **382**, 698 (2023).
[23] M. Hamada, E. Minamitani, M. Hirayama, and S. Murakami, Phys. Rev. Lett. **121**, 175301 (2018).
[24] S. Streib, H. Keshtgar, and G. E. W. Bauer, Phys. Rev. Lett. **121**, 027202 (2018).
[25] K. An, A. N. Litvinenko, R. Kohno, A. A. Fuad, V. V. Naletov, L. Vila, U. Ebels, G. de Loubens, H. Hurdequint, N. Beaulieu, J. Ben Youssef, N. Vukadinovic, G. E. W. Bauer, A. N. Slavin, V. S. Tiberkevich, and O. Klein, Phys. Rev. B **101**, 060407(R) (2020).
[26] A. Rückriegel and R. A. Duine, Phys. Rev. Lett. **124**, 117201 (2020).
[27] R. M. Geilhufe and W. Hergert, Phys. Rev. B **107**, L020406 (2023).
[28] Y. Ren, C. Xiao, D. Saparov, and Q. Niu, Phys. Rev. Lett. **127**, 186403 (2021).
[29] H. Katsura, A. V. Balatsky, and N. Nagaosa, Phys. Rev. Lett. **98**, 027203 (2007).
[30] X.-W. Zhang, Y. Ren, C. Wang, T. Cao, and D. Xiao, Phys. Rev. Lett. **130**, 226302 (2023).
[31] F. Wu, S. Bao, J. Zhou, Y. Wang, J. Sun, J. Wen, Y. Wan, and Q. Zhang, Nat. Phys. **19**, 1868 (2023).

[32] A. Kamra, H. Keshtgar, P. Yan, and G. E. W. Bauer, Phys. Rev. B **91**, 104409 (2015).
[33] A. Kamra and G. E. Bauer, Solid State Commun. **198**, 35 (2014).
[34] M. Weiler, H. Huebl, F. S. Goerg, F. D. Czeschka, R. Gross, and S. T. B. Goennenwein, Phys. Rev. Lett. **108**, 176601 (2012).
[35] B. Flebus, K. Shen, T. Kikkawa, K.-I. Uchida, Z. Qiu, E. Saitoh, R. A. Duine, and G. E. W. Bauer, Phys. Rev. B **95**, 144420 (2017).
[36] T. Kikkawa, K. Shen, B. Flebus, R. A. Duine, K.-I. Uchida, Z. Qiu, G. E. W. Bauer, and E. Saitoh, Phys. Rev. Lett. **117**, 207203 (2016).
[37] A. Rückriegel, P. Kopietz, D. A. Bozhko, A. A. Serga, and B. Hillebrands, Phys. Rev. B **89**, 184413 (2014).
[38] See Supplemental Material at http://link.aps.org/supplemental/10.1103/PhysRevB.110.024423 for our discussion of the existence of phonon magnetic moments in kagome and square lattices.
[39] G. Go, S. K. Kim, and K.-J. Lee, Phys. Rev. Lett. **123**, 237207 (2019).
[40] E. Thingstad, A. Kamra, A. Brataas, and A. Sudbø, Phys. Rev. Lett. **122**, 107201 (2019).
[41] S. Zhang, G. Go, K.-J. Lee, and S. K. Kim, Phys. Rev. Lett. **124**, 147204 (2020).
[42] C. Kittel, Phys. Rev. **110**, 836 (1958).
[43] C. Kittel, Rev. Mod. Phys. **21**, 541 (1949).
[44] J. Bonini, S. Ren, D. Vanderbilt, M. Stengel, C. E. Dreyer, and S. Coh, Phys. Rev. Lett. **130**, 086701 (2023).
[45] S. Ren, J. Bonini, M. Stengel, C. E. Dreyer, and D. Vanderbilt, Phys. Rev. X **14**, 011041 (2024).
[46] X.-Y. Chen and Y.-P. Wang, Phys. Rev. B **104**, 155132 (2021).
[47] S. Liu, M.-Q. Long, and Y.-P. Wang, Phys. Rev. B **108**, 184414 (2023).
[48] S. Liu, M.-Q. Long, and Y.-P. Wang, Nano Lett. **23**, 7427 (2023).